X-ray magnetic circular dichroism in the near and extended absorption edge structure (invited)

G. Schütz, P. Fischer, and K. Attenkofer
Institute für Experimental Physics II, University Augsburg, D 86135 Augsburg, Germany

M. Knülle, D. Ahlers, S. Stähler, and C. Detlefs
Physics Department E12, Technical University Munich, D 85747 Garching, Germany

H. Ebert
Institute für Physical Chemistry, University of Munich LMU, D 80333 Munich, Germany

F. M. F. de Groot
L.U.R.E, Bât. 209D, F 91405 Orsay, France

Magnetic circular dichroism (MCD) studies at K and L edges using hard and soft x rays are presented. The relation of this universal phenomenon in the x-ray absorption near-edge structure (XANES) and extended x-ray absorption fine structure (EXAFS) regions to local magnetic structures in the case of $3d$ and $4f$ elements is illustrated. The validity of atomic and band-structure pictures to describe the MCD in the XANES range are outlined and the applicability of sum rules and two-step vector coupling models to deduce spin and orbital moments of the absorbing atom as well as spin-density profiles from the experimental data are critically discussed. The correlation of the dichroic contribution in the EXAFS to the magnetic moments and spin densities of the neighboring atoms are addressed by systematic studies which provide new insights into the exchange phenomena of the interaction of spin-polarized electrons with ferromagnetic media. The potential but also the limitations of this new spectroscopy is demonstrated.

I. INTRODUCTION

X-ray circular magnetic dichroism (X-MCD) in core-to-valence transitions is a new powerful method to study in an element- and symmetry-selective manner the magnetic aspects of local electronic structures in magnetic media. The possibility of extracting local spin and orbital moments using "sum rules" deduced on the basis of an atomic approach[1,2] or in the local spin-density (LSD) formalism[3,4] by a comparison of the magnetic L_2- and L_3-dichroic spectra is one of the dominant subjects of interest. To date a correct interpretation of experimental spectra seems to be restricted to cases with either a localized character of the involved final states as, e.g., $3d$-$4f$ transitions in rare earth (RE) systems,[5,6] where an atomic picture[7] is adequate or to those with a delocalized behavior as, e.g., $1s$-$4p$ transitions in $3d$ elements and $2s$-$6p$ transitions in $4f/5d$ systems[8,9] and $2p$-$5d$ transitions in $5d$ elements,[3] where the band-structure approach has been adopted successfully.[10] For intermediate cases, however, as the $L_{2,3}$ edges in transition elements[5,11] and in REs,[9,12] a closed theoretical description is still a problem.

Although the occurrence of a dichroic contribution to the extended (EXAFS) [spin-polarized EXAFS (SPEXAFS)] has been proven to be a universal phenomenon,[4,13] theoretical calculations of the experimental spectra are not available but are on the way.[14] However, as demonstrated in the second part of this article, the systematics observed in several systems show that on the basis of simple two-step models interesting correlations of the SPEXAFS to the local magnetic short-range order can be found, which demonstrate the potential of this method to study magnetic structures on an atomic scale.

II. NEAR-EDGE MCD

A. Theoretical models

Large MCD effects (in some cases more than 20%) are found in the near-edge region within 20 eV above an absorption threshold. In this energy range the absorption cross section can be described by Fermi's golden rule.[15] In the case of bandlike final states, the single-particle density-of-states model describes the experimental spectra successfully. The energy dependence of the absorption cross section is given by the density profile of the final states with selected symmetry determined by dipole-selection rules times a nearly energy-independent matrix element. If the final states are well localized, two-particle interactions have to be included. These can be calculated explicitly using atomic multiplet[16] approaches. Here it is also possible to include solid state effects by adding crystal field terms to the Hamiltonian and hybridization of ligand character by an admixture of extra-atomic configurations such as in charge-transfer states.

In both cases, polarization effects and exchange splittings can be taken into account. Using fully relativistic spin-polarized Korringa–Kohn–Rostoker (KKR)–GF and linear muffin-tin orbital[10] band-structure approaches or spin-polarized versions of the linear augmented plane wave (LAPW) method,[7] the MCD L spectra of various heavier

 0021-8979/94/76(10)/6453/6/$6.00

transition metals such as magnetic $5d$ elements and Gd-metal have been successfully described in the single-particle picture, while on the other hand the experimental $M_{4,5}$-MCD spectra in RE systems are excellently reproduced by atomic calculations.[6]

On the basis of the atomic description sum rules have been developed recently,[1,2] which relate the difference and the sum of the dichroic signals ($\mu^{\pm}$) for reversed photon polarization $\mu_c := (\mu^+ - \mu^-)/2$ for the two spin-orbit initial states directly to the local spin and orbital moments of the partially filled final valence shell.

Based on a simple vector-coupling version of the band-structure approach, a similar relation between the normalized MCD spectra μ_c/μ_0 at the L_2 and L_3 edges times the unoccupied final state density and the local magnetic moments can be deduced.[4,9] Based on the Fano effect[8] the sensitivity of the dichroic signal to the spin and orbital moment originates from finite spin $\langle \sigma_z \rangle$ and orbital polarization $\langle l_z \rangle$ of the outgoing photoelectron in the propagation direction z of the circularly polarized photon. The photoelectron emitted from an unpolarized core state is thus considered as a polarized probe for the spin and orbital moment of the final states. The polarization values for a free electron wave are $\langle l_z \rangle = +3/4$ in an initial p state and $\langle \sigma_z \rangle = -1/2$ and $+1/4$ for the corresponding $p_{1/2}$ and $p_{3/2}$ spin-orbit partners.

In a simple spin-polarized version of Fermi's golden rule for pure spin-ferromagnetic systems,[8,9] the MCD signal is directly correlated to the spin density $\Delta\rho = \rho^+ - \rho^-$ of the final state by $[\mu_c/\mu_0](E) = \langle \sigma_z \rangle [\Delta\rho/\rho](E)$, which corresponds to $\mu_c(E) \sim -\Delta\rho(E)$ at the L_2 and $\mu_c(E) \sim +\Delta\rho(E)$ at the L_3 edges for $\mu_0(L_3) = 2\mu_0(L_2)$.[9]

Within the vector-coupling model the relation between the normalized MCD spectra μ_c/μ_0 and the spin and orbital moments is deduced to

$$\mu_S/\mu_B \sim -\tfrac{4}{3} \int \{[\mu_c/\mu_0]_{L_3}(E) - [\mu_c/\mu_0]_{L_2}(E)\} \rho(E) dE, \tag{1}$$

$$\mu_L/\mu_B \sim -\tfrac{4}{9} \int \{[\mu_c/\mu_0]_{L_3}(E) + 2[\mu_c/\mu_0]_{L_2}(E)\} \rho(E) dE. \tag{2}$$

Under the condition $\mu_0(L_3) = 2\ \mu_0(L_2)$ Eqs. (1) and (2) are equivalent to the sum rules, which are more appropriate in case of (nearly) isolated absorption profiles (white lines =WL) as, e.g., the $M_{4,5}$ edges in RE, while Eqs. (1) and (2) can be more easily applied in the case of more steplike absorption edges, e.g., the $L_{2,3}$ edges in heavier elements, without or with weakly indicated WL structure as in some RE and Pt and Au systems.

For K edges $\langle l_z \rangle$ amounts -1 and $\langle \sigma_z \rangle$ has the very small value of $\sim 10^{-2}$. Thus only weak MCD effects of less than 1% are expected for outer, bandlike final states with nearly quenched orbital moments, as, e.g., the $(4)p$ states in $3d$ elements or $(6)p$ in $4f/5d$ systems and no simple relation of the MCD profile and the local p moment exists.

B. Fe-metal layers

To demonstrate the reliability of the sum rules Eqs. (1) and (2), they are applied to $L_{2,3}$ MCD spectra of Fe-metal layers (cf. Fig. 1). The exact thicknesses of the 9.25 Å (A) and 24 Å (B) Fe layers (deposited on 300 Å Au on a glass substrate and protected by a 30 Å Al coverlayer) and the magnetic moments per atom of 2.07(3) μ_B for the thin (A) and 2.14(3) μ_B for the thicker sample (B) were determined via XFA and super conducting quantum interference device (SQUID) measurements, respectively.[20] The μ_c profiles are shown in Fig. 1(a) in addition to the spin-averaged μ_0 profile for the 9.25 Å (dashed line) and the 24 Å Fe layers (solid line). Corresponding theoretical spectra from fully relativistic spin polarized KKR calculation for iron metal are presented in Fig. 1(b).[10] The experimental data measured by total-yield detection in an applied external field of 0.2 T were taken at the DRAGON beamline (NSLS).

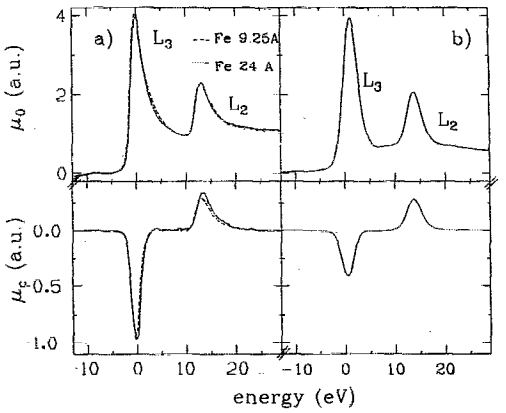

FIG. 1. Experimental absorption and dichroic profiles (a) at the Fe $L_{2,3}$ edges of Fe metal layers with thicknesses of 9.25 Å (dashed) and 24 Å (solid) in comparison with theoretical profiles from band-structure calculations (b). The experimental spectra correspond to raw and unsmoothed data with subtracted linear background.

Figure 1(a) shows, that the dichroic L_2 signal is significantly reduced relative to the L_3 signal causing a strong deviation from the ratio $\mu_c(L_2)/\mu_c(L_3) = -1$ expected for pure spin moments. This indicates the existence of an orbital moment coupled parallel to the spin moment [Eq. (4)]. Applying the sum rules one deduces a spin and orbital moment of $m_S \sim 2.19\mu_B$ $(2.29\mu_B)$ and $m_L \sim 0.25\mu_B$ $(0.21\mu_B)$ for samples A (B) taking into account $n = 4$ holes in the $3d$ level. The errors of these numbers due to the uncertainties of estimating the white line areas amounts to 20%. Very similar, somewhat smaller values of $m_S \sim 2.02\mu_B$ $(2.08\mu_B)$ and $m_L \sim 0.20\mu_B$ $(0.15\mu_B)$ (uncertainty about 5%) are found by applying Eqs. (3) and (4) using theoretical density of states profiles with an integrated value of $\int \rho(E) = 3.1$. These results are in excellent agreement with the results of the macroscopic measurements and confirm the expected increase of m_L with decreasing layer thickness.

Only the absolute values of m_L are larger than expected from theory and other measurements.[21] The spin polarized KKR calculation of the μ_0 and μ_c spectra seems to underestimate the values of μ_c and μ_0 at the L_2 edges, which could be an indication for the breakdown of the single-particle approach, as has been found for the $L_{2,3}$ MCD in the lighter $3d$ transition metals.

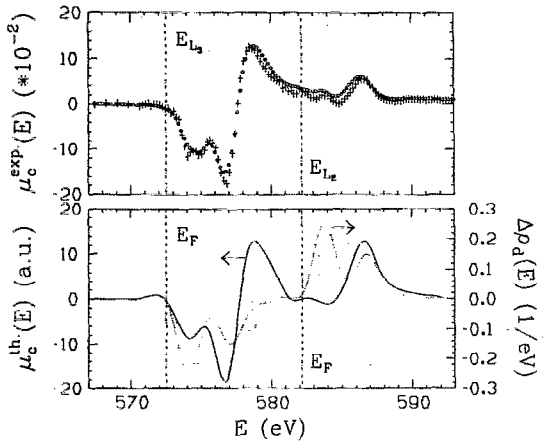

FIG. 2. Top: experimental dichroic absorption of CrO_2 at the L_3 and L_2 edges of chromium, measured at the SX700/3 (BESSY) (O) and DRAGON beamlines (NSLS) (+) with energy resolutions of about 900 and 500 meV, respectively. From the raw data only a constant offset has been subtracted. Bottom: theoretical dichroic absorption at the L_3 and L_2 edge of CrO_2, given by LMTO calculation (—) and the spin density of the $3d$ band above the Fermi level, given by LAPW band-structure calculations. The L_2 edge is rescaled by (-1) due to the negative photoelectron polarization. The vertical lines (---) mark the energy of the L_2 and L_3 edges, which are identical to the Fermi levels of the plotted spin densities.

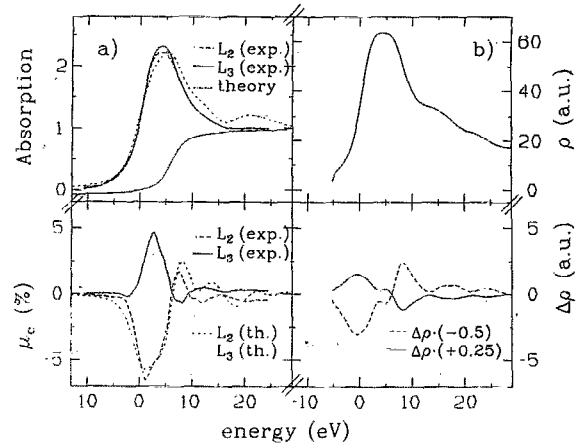

FIG. 3. (a) Experimental L_2 (dashed) and L_3 (solid) absorption (μ_0) (top) and corresponding dichroic profiles (μ_c) (bottom) of Gd-metal in comparison with theoretical unpolarized (dash-dotted) (top) and L_2 (dash-dotted), L_3 (dots) polarized profiles (bottom). The first inflection point of the absorption onset is chosen as the origin of the energy scale. The experimental absorption step is fitted by an arctan function (width 4 eV). (b) Theoretical total d spin-density profiles ($\rho=\rho^+ + \rho^-$) (top) and corresponding difference (b) ($\Delta\rho=\rho^+ - \rho^-$) broadened by core hole lifetime and experimental resolution and rescaled by -0.5 and $+.25$ at the $L_{2,3}$ edges, respectively. The dash-dotted line represents the theoretical MCD profile.

C. Cr $L_{2,3}$ MCD spectra

Going to lower Z within the $3d$ series due to the decrease of the $2p$ spin-orbit splitting below 10 eV it is difficult to separate the corresponding L_2 and L_3 parts in the spectra as seen in case of the Cr MCD in the half-metallic ferromagnet CrO_2 presented in Fig. 2. The dichroic profile is much more complex than in the heavier transition metals and even changes sign within the L_3 contribution. A comparison with the calculation of the dichroic effects for transition metal ions in the atomic approach[22] suggests that these models are more appropriate to reproduce the experimental findings and thus we have used a ligand field multiplet model (LFM), which includes the influence of the cubic crystal field on the local wave functions.[23] Setting the spin-orbit splitting to zero gives a reasonably good agreement between theory indicating the validity of the theoretical concept for the description of the MCD effects. The vanishing influence of an orbital momentum and correlated spin-orbit effects can also be verified by the application of the sum rules, which gives an upper limit of m_L of less than $10^{-2}\mu_B$. It can also be seen from the MCD spectra that it is difficult to deduce the corresponding spin moment in case of too close, i.e., not well resolved, $L_{2,3}$ absorption edges. That the LSD approach and the model Eqs. (1) and (2) are based on fails can be demonstrated by a comparison of the local unoccupied spin density of states $\Delta\rho$ shifted to the absorption edge with the μ_c profile, which show only rather poor similarities.

D. $L_{2,3}$ MCD in Gd-metal and $Eu_3Fe_5O_{12}$

Dichroic $L_{2,3}$ effects of several percent in REs have been found in all systems investigated up to now. Theoretical descriptions, however, have concentrated on Gd, as the fully relativistic band-structure approach by Ebert[10] and the calculations carried out by Carra *et al.*[17] which were also extrapolated to heavier RE metals.

However the description of the REs with nonzero $4f$ angular momentum is still an open problem. In particular the structures at the L_3 edges at negative energies, characteristic for all systems except Gd, have been proven to exhibit an atomic character.[24]

Although the ratios of the normalized Gd $L_{2,3}$ MCD profiles (both peak values and integrated areas) as seen in Fig. 3 are close to -2, i.e., the ratio of the spin-polarization factors, applying the sum rules Eqs. (1) and (2) leads to a spin moment of $-0.24\mu_B$ having the opposite sign compared to the theoretical calculations, which predict $\mu_S=+0.47\mu_B$ for the spin and $\mu_L=-0.04\mu_B$ for the orbital d moment.[25] The sum rules yield for the orbital moment a value of $-0.004\mu_B$ which is a factor of 10 too small compared with the theoretical prediction. Similar results are obtained even in the naive vector-coupling model ($\mu_S=-0.19\mu_B$ and $\mu_L=-0.002\mu_B$).

A direct comparison of the unbroadened theoretical Gd MCD profiles with unbroadened spin densities (Fig. 4) explains the breakdown of the validity of the basic assumptions Eqs. (1)–(2) are based on. Though the fine structures of the profiles coincide roughly, indicating a direct correlation between μ_c/μ_0 and $\Delta\rho/\rho$, the value of $\langle\sigma_z\rangle$ obviously becomes strongly energy dependent, amounting, e.g., to a value twice as high at the Fermi energy. Hence the small positive spin density leads to a strong line in the $L_{2,3}$ MCD spectrum at E_F and a negative spin moment.

The physical origin is a strong energy and spin dependence of the matrix element, since close to E_F the overlap of initial and final spin-up wave functions is much larger for the

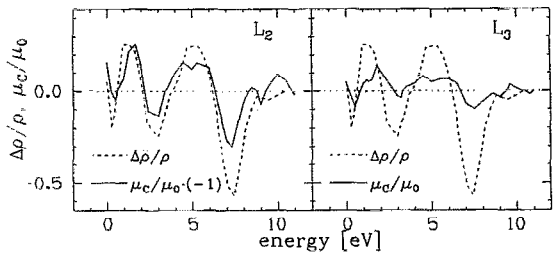

FIG. 4. Unbroadened theoretical $\Delta\rho/\rho$ profiles (dashed) and unbroadened theoretical μ_c/μ_0 profiles (solid) at the L_2 (left) and L_3 (right) edges in Gd-metal. The ratio $(\Delta\rho/\rho)/(\mu_c/\mu_0)$ is not constant with energy.

corresponding states of minority character, a fact, which has to be neglected in the models. But the MCD calculations (shown in Fig. 3) using the single particle band-structure approach reproduces this behavior exactly.

Applying the sum rules in the case of Eu $L_{2,3}$ MCD spectra (Fig. 5) in $Eu_3Fe_5O_{12}$ yields a spin moment of $-0.03\mu_B$ and an orbital moment of $+0.005\mu_B$. The moments obtained in the naive vector-coupling model amount to $-0.03\mu_B$ for the spin and $+0.007\mu_B$ for the orbital contribution. However, similar to Gd, these values lead to the wrong sign for the spin, which can again be drawn back to matrix-element effects. On the other hand, the expected opposite signs of μ_L and μ_S, induced in the $5d$ state by the intra-atomic $4f$-$5d$ coupling in lighter REs, seems to be directly manifested in the collapse of the L_3 MCD to the credit of a strong L_2 dichroic signal.

III. MAGNETIC EXAFS

A. Theoretical aspects

A phenomenological description of the measured effects is presented based on the simple vector-coupling "two-step" model, which has successfully been used to describe the near-edge MCD in the "spin-only" limit. In the first step, we assume that a free electron wave is going out with a spin

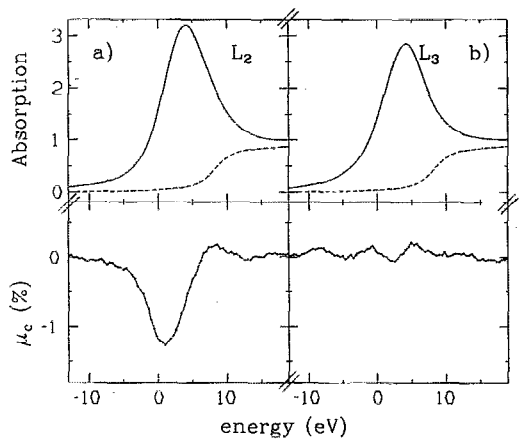

FIG. 5. (a) Experimental L_2 (a), L_3 (b) absorption (μ_0) (top) and dichroic profiles (μ_c) (bottom) of Eu in $Eu_3Fe_5O_{12}$. The absorption step is fitted by an arctan function (width 4 eV).

projection $\langle\sigma_z\rangle$ in photon-beam direction. If the magnetic moment of the neighboring atom, i.e., the spin of its majoritylike electrons, is also polarized in z direction, an exchange contribution to the Coulomb scattering potential is present in the scattering processes of the outgoing photoelectron. This should result in a magnetic contribution to the backscattering amplitude, which changes its sign with reversing the relative orientation of the photoelectron spins and the spins of the magnetic neighbors in the absorption process. In the conventional EXAFS formula the effect of exchange interaction in the scattering process is described by an additive exchange contribution (with index c) to the Coulomb-interaction parameters, i.e., the backscattering amplitude $F=F_0\pm F_c$, the phase shift $\phi=\phi_0\pm\phi_c$ and the mean free path $\lambda=\lambda_0\pm\lambda_c$. The strengths of the exchange contribution are within this simple model expected to scale directly with the spin-polarization parameter, i.e., $\langle\sigma_z\rangle\sim F_c$, ϕ_c, λ_c.

Thus the conventional EXAFS (χ_0)[41] as function of the photoelectron de-Broglie wave-number k, which are described by a summation over the coordination shells located at distances r_j with N_j neighboring atoms and including the Debye–Waller factor D_j and "shake-off/on" processes at the central atom i (S_i), is transferred into a spin-polarized expression $\chi_c=\chi^+-\chi^-$ by

$$\chi_c(k)=\sum_j N_jS_i(k)D_j(k)\frac{e^{-2r_j/\lambda_{jo}}}{kr_j}\left(F_{jc}\sin(2kr_j+\varphi_{ijo})+\varphi_{ijc}F_{jo}\cos(2kr_j+\varphi_{ijo})+\frac{2r_j\lambda_{jc}}{\lambda_{jo}^2}F_{jo}\sin(2kr_j+\varphi_{ijo})\right). \quad (5)$$

B. Experimental results

1. $L_{2,3}$ SPEXAFS

SPEXAFS studies in the hard x-ray range have been performed in the transmission mode at HASYLAB (Hamburg) in various magnetic systems at the L edges in REs and $5d$ elements and at the K edges of $3d$ systems.[4]

For an analysis of the EXAFS and accordingly of the SPEXAFS to deduce structural information as, e.g., the distances r_j of next atoms and the coordination numbers N_j a sufficiently extended range of the $\chi_{0/c}$ spectra is Fourier transformed. Thus, this method is often not well practicable for energetically close following $L_{2,3}$ edges in $3d$ elements. This holds especially for the SPEXAFS analysis, since according to the simple picture the magnetic oscillation at the L_2 and L_3 edges should show identical structures but with opposite sign, which is found in all systems studied up to now as demonstrated in Fig. 6 at the Eu $L_{2,3}$ edges in the ferromagnetic Eu iron garnet ($Eu_3Fe_5O_{12}$).

If one takes into account a ratio of the amplitudes of -2, the χ_c profiles at the L_2 and L_3 edges are identical. The corresponding near-edges MCD signals (Fig. 5), behave completely different due to their dependence on the orbital moment. This proves that similar effects of the orbital polarizations can be neglected in the SPEXAFS interpretation. Only an additional contribution due to the small near-edge MCD at the iron K edge causes some deviation at the L_3

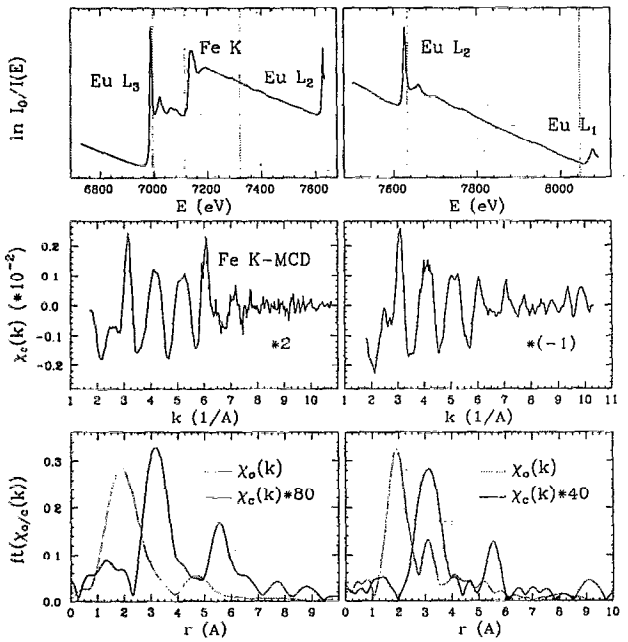

FIG. 6. Top: the absorption of $Eu_3Fe_5O_{12}$ between 6700 and 7680 eV (left) and between 7480 and 8120 eV (right), displaying the Fe K and the Eu L_3, L_2, and L_1 edges. Center: the SPEXAFS at the Eu L_3 (left) and L_2 edge (right) follow the same profile with a ratio of (−2). Bottom: the Fourier transform of the spin-averaged EXAFS (···) and SPEXAFS (—) of the Eu L_3 (left) and L_2 edge (right).

edge ($k=6$ Å^{-1}). Since in the simple picture the corresponding K-edge SPEXAFS are more than one order of magnitude smaller, they are nearly invisible in the L_3 SPEXAFS.

The Fourier transform (FT) of the polarization averaged EXAFS spectrum $f(\chi_0)$ (dashed line) and the corresponding SPEXAFS FT (solid line) $f(\chi_c)$ are significantly different. The FT of the L_3 EXAFS show very broad features due to the small transformation range limited by the Fe K edge. The prominent maximum in $f(\chi_o)$ resulting from the strong backscattering at the next oxygen neighbors has vanished in the SPEXAFS to the credit of an increase of the peaks at higher r values, which mark the positions of the next and over next iron Fe neighbors. They are small or almost invisible in the EXAFS FT. The $f(\chi_c)$ at the L_2 and L_3 edges are very similar demonstrating that the occurrence of the Fe K edge does not limit the k range in the magnetic spectra.

These studies show, that (nearly) nonmagnetic neighbors as the oxygen components on magnetic oxides do not contribute to the SPEXAFS and a clear distinction between magnetic and nonmagnetic neighborhood is possible. From the systematics observed by studies in various systems,[4,13] we have observed that the relative strength of the SPEXAFS rescaled by the photoelectron spin polarization

$$[\chi_c/\chi_0]/\langle\sigma_z\rangle=[f(\chi_c)/f(\chi_o)]\langle\sigma_z\rangle=2.4(3)\%\mu_S(\mu_B) \tag{6}$$

is directly proportional to the magnetic spin moment of the neighboring atoms. Thus, we expect, that the SPEXAFS spectroscopy gives even quantitatively new element-specific insights into the magnetic short-range order.

2. K-edge SPEXAFS

The highly precise measurements, which are possible in the transmission mode, allow us also to address $3d$ elements by K-edge SPEXAFS studies as demonstrated in case of Co-(fcc) and Ni-metal. As shown in Fig. 7, the χ_c oscillation at the K edges follow roughly the χ_0 structure except an additional contribution at a k region of 4–5 Å^{-1}. In this range multielectron contributions ($3p\rightarrow 3d$ transition) result in an additional line in the dichroic K spectra, which decreases strongly by going from Fe to Ni.[13] Following Eq. (6), we deduce a value of $\langle\sigma_z\rangle=+3.5(5)\%$ for the K SPEXAFS, which is somewhat larger than expected from the near-edge MCD effects.

Due to the small value of $\langle\sigma_z\rangle$ the statistics of the K SPEXAFS can be poor. But a more detailed analysis by an extraction of the exchange parameter from the experimental data allows also in this case a sufficiently quantitative analysis. Hereby the values F_{jo}, ϕ_{ijo}, and λ_{jo} are calculated by the FEFF code of Rehr[17] and the D_j and S_i values can be deduced by fitting the χ_o profiles. The F_c profile for Co and Ni indicate a significant different k dependence of the magnetic and Coulomb backscattering amplitude F_o, which seems to be correlated to the differences of the distribution of spin and charge density in the neighboring atom. The ratio of the Co and Ni F_c amplitudes scale directly with the ratio of the magnetic moments per atom. Thus the described analysis allows the determination of the average magnetic moment carried by a coordination shell with good accuracy even for noisy SPEXAFS data.

The amplitudes of F_c correspond to relatively large exchange contributions of the *elastic* scattering cross section of more than 20% per magnetic electron. On the other hand the

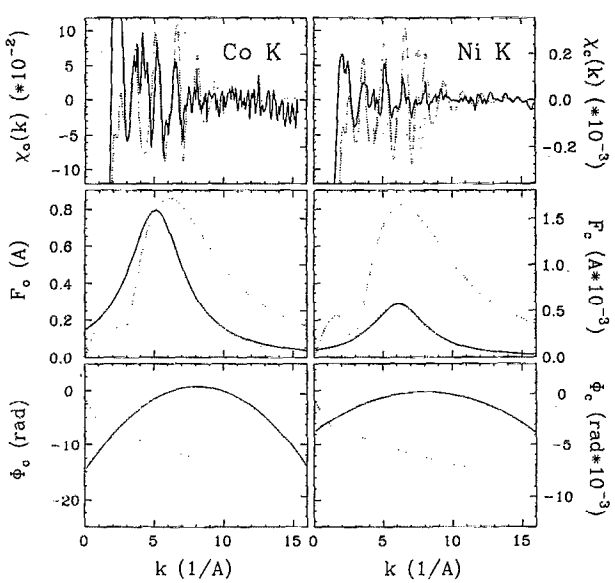

FIG. 7. Top: the EXAFS (···) and SPEXAFS (—), measured at the Co K (left) and Ni K edge (right) of Co fcc and Ni fcc metal. Center: the calculated spin-independent (···) and fitted spin-dependent part (—) of the backscattering amplitude of the first neighbor of Co fcc (left) and Ni fcc (right). Bottom: the corresponding calculated spin-independent (···) and fitted spin-dependent (—) phase shift.

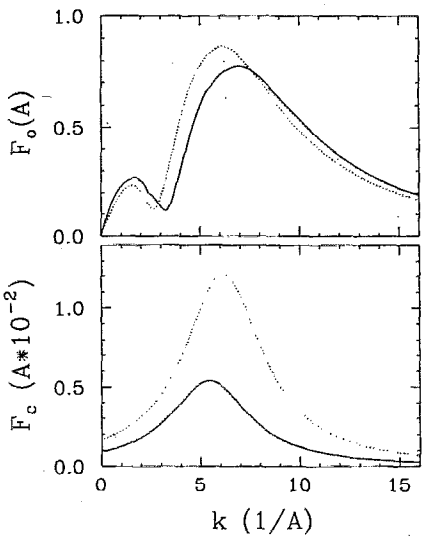

FIG. 8. The calculated spin-independent part F_0 (top) and fitted spin-dependent part F_c (bottom) of the backscattering amplitude for Co (···) and Cu (—) of a Co(5) Cu(4) multilayer.

exchange contributions to the phase shift, as seen from Fig. 7, are much smaller and the spin-dependent mean-free path of the order of less than 10^{-3} is found to be negligible. This demonstrates that the SPEXAFS analysis can also provide useful new information on the exchange phenomena in the interaction of spin-polarized electrons directly inside a solid and especially in comparison with corresponding results from surface-sensitive electron spectroscopies.

SPEXAFS studies can be applied even for multilayered systems (ML) to get information on the interface structures, as shown for Co/Cu systems. Our calculated distribution of the magnetic moments of 5Co/4Cu ML (Fig. 9) indicates a small Cu polarization corresponding to an average spin and orbital moment of $m_S(\mathrm{Cu})=0.0137\mu_B$ and $m_L=0.001\mu_B$, which agree well to our near-edge MCD studies at the NSLS, where we observed for the first time an induced Cu moment in this ML of $m_S(\mathrm{Cu})=0.014\mu_B$ and $m_L<0.002\mu_B$.[4]

In MLs with strongly different magnetic moments of both components as the Co/Cu systems the average magnetic moments of the *neighboring* Co and Cu atoms depend very sensitively on the sharpness of the interface. The ratio between the Co and Cu SPEXAFS amplitudes resulting from the exchange scattering at the first coordination shell should be about 7.3 for a sharp interface and reduced to ~1.9 for a complete intermixing of two adjacent atomic layers. Thus a comparison of the strengths of F_c deduced from the Co and Cu SPEXAFS in the ML (see Fig. 8) gives quantitative information on the quality of the interface. Their ratio of the amplitudes of ~2.0 are significantly smaller than the value of 7.3 estimated for an ideal structure and can be explained by an intermixing of close to 50% in the first Co and Cu at the interface.

ACKNOWLEDGMENTS

We would like to thank all colleagues involved in this work, G. Bayreuther, S. Parkin, J. Stöhr, A. Fontaine, C. T. Chen, H. Petersen , K. Schwarz, and P. Blaha. The help of the staffs at TU Munich, the University of Augsburg, at HASYLAB, BESSY, and NSLS is appreciated. This work is supported by the German Federal Minister of Research and Technology (BMFT) under Contract No. 05 5WO EAI.

[1] B. T. Thole, P. Carra, F. Sette, and G. van der Laan, Phys. Rev. Lett. **68**, 1943 (1992).
[2] P. Carra, B. T. Thole, M. Altarelli, and X. Wang, Phys. Rev. Lett. **70**, 694 (1993).
[3] R. Wienke, G. Schütz, and H. Ebert, J. Appl. Phys. **69**, 6147 (1991).
[4] G. Schütz, M. Knülle, and H. Ebert, Phys. Scr. **T49**, 302 (1993).
[5] F. Sette, C. T. Chen, Y. Ma, S. Modesti, and N. V. Smith, *Proceedings of 6th International Conference on X-ray Absorption Fine Structure*, edited by S. Samar Hasnain (Horwood, Chichester, UK, 1991), p. 96.
[6] J. Ph. Schillé, J. P. Kappler, Ph. Sainctavit, Ch. Cartier dit Moulin, C. Brouder, and G. Krill, Phys. Rev. B **48**, 9491 (1993).
[7] B. T. Thole, G. van der Laan, and G. A. Sawatzky, Phys. Rev. Lett. **55**, 2086 (1985).
[8] G. Schütz, W. Wagner, W. Wilhelm, P. Kienle, R. Zeller, R. Frahm, and G. Materlik, Phys. Rev. Lett. **58**, 73 (1987).
[9] G. Schütz, M. Knülle, R. Wienke, W. Wilhelm, W. Wagner, P. Kienle, and R. Frahm, Z. Phys. B **73**, 67 (1988).
[10] H. Ebert, P. Strange, and B. L. Gyorffy, J. Phys. Condens. Matter B **73**, 77 (1988); H. Ebert, B. Drittler, R. Zeller, and G. Schütz, Solid State Commun. **69**, 485 (1989); H. Ebert, G. Schütz, and W. M. Temmerman, Solid State Commun. **76**, 475 (1990).
[11] C. T. Chen, F. Sette, Y. Ma, and S. Modesti, Phys. Rev. B **42**, 7262 (1990); Y. U. Idzerda, L. H. Tjeng, H. J. Lin, G. Meigs, C. T. Chen, and J. Gutierrez, J. Appl. Phys. **73**, 6204 (1993).
[12] P. Fischer, G. Schütz, and G. Wiesinger, Solid State Commun. **76**, 777 (1990); P. Fischer, G. Schütz, S. Stähler, and G. Wiesinger, J. Appl. Phys. **69**, 6144 (1991).
[13] G. Schütz, R. Frahm, P. Mautner, R. Wienke, W. Wagner, W. Wilhelm, and P. Kienle Phys. Rev. Lett. **62**, 2620 (1989); M. Knülle, D. Ahlers and G. Schütz, Solid State Commun. (to be published).
[14] J. J. Rehr (private communication, 1994).
[15] J. C. Fuggle and J. E. Inglesfield, *Unoccupied Electronic States*, edited by J. C. Fuggle (Springer, Berlin, 1992).
[16] B. T. Thole, G. van der Laan, and P. H. Butler, Chem. Phys. Lett. **149**, 295 (1988).
[17] P. Carra, B. N. Harmon, B. T. Thole, M. Altarelli, and G. A. Sawatzky, Phys. Rev. Lett. **66**, 2495 (1991).
[18] U. Fano, Phys. Rev. **178**, 131 (1969).
[19] J. L. Erskine and E. A. Stern, Phys. Rev. B **12**, 5016 (1975).
[20] M. Knülle, G. Schütz, G. Bayreuther, and C. T. Chen, Solid State Commun. (to be published).
[21] P. Söderlind, O. Eriksson, B. Johansson, R. C. Albers, and A. M. Boring, Phys. Rev. B **45**, 12 911 (1992).
[22] G. van der Laan and B. T. Thole, Phys. Rev. B **43**, 13 401 (1991).
[23] F. M. F. de Groot, J. C. Fuggle, B. T. Thole, and G. A. Sawatzky, Phys. Rev. B **42**, 5459 (1990).
[24] P. Fischer, G. Schütz, S. Scherle, M. Knülle, S. Stähler, and G. Wiesinger, Solid State Commun. **82**, 857 (1992).
[25] J. Sticht and J. Kübler, Solid State Commun. **53**, 529 (1985).
[26] B. K. Teo, in *EXAFS Spectroscopy*, edited by D. C. Joy (Plenum, New York, 1981).
[27] J. J. Rehr, S. I. Zabinski, and R. C. Albers, Phys. Rev. Lett. **69**, 3397 (1992).